

K-shell dielectronic resonances in photoabsorption: differential oscillator strengths for Li-like C IV, O VI, and Fe XXIV

Sultana N. Nahar and Anil K. Pradhan

Department of Astronomy, The Ohio State University, Columbus, Ohio 43210

Hong Lin Zhang

Applied Theoretical and Computational Physics Division, Los Alamos national Laboratory, Los Alamos, NM 87544
(November 1, 2018)

Recently X-ray photoabsorption in KLL resonances of O VI was predicted [Pradhan, *Astrophys. J. Lett.* **545**, L165 (2000)], and detected by the *Chandra X-ray Observatory* [Lee *et al.*, *Astrophys. J. Lett.*, in press]. The required resonance oscillator strengths, \bar{f}_r , are evaluated in terms of the differential oscillator strength $df/d\epsilon$ that relates bound and continuum absorption. We present the \bar{f}_r values from radiatively damped and undamped photoionization cross sections for Li-like C, O, and Fe calculated using relativistic close coupling Breit-Pauli R-matrix method. The KLL resonances of interest here are: $1s2p(^3P^o)2s$ [$^4P_{1/2,3/2}^o, ^2P_{1/2,3/2}^o$] and $1s2p(^1P^o)2s$ [$^2P_{1/2,3/2}^o$]. The KLL photoabsorption resonances in Fe XXIV are fully resolved up to natural autoionization profiles for the first time. It is demonstrated that the undamped \bar{f}_r independently yield the resonance radiative decay rates, and thereby provide a precise check on the resolution of photoionization calculations in general. The predicted photoabsorption features should be detectable by the X-ray space observatories and enable column densities in highly ionized astrophysical plasmas to be determined from the calculated \bar{f}_r . The dielectronic satellites may appear as redward broadening of resonance lines in emission and absorption.

PACS number(s): 34.80.Kw, 32.80.Dz, 32.80.Fb

Resonance spectroscopy may be employed to determine element abundances and ionization structure in astrophysical sources [1,2]. K-shell line spectra are powerful diagnostic tools in X-ray spectroscopy for density, temperature, ionization state, and abundances laboratory and astrophysical plasmas (e.g. [3,4]). K-shell emission spectra from several atomic species have been measured in Electron-Beam-Ion-Trap experiments [3,5]. Recently it was suggested that, analogous to the dielectronic satellite spectra of He-like ions in emission, K-shell X-ray photoabsorption should be detectable in KLL resonances of Li-like O VI [1]. Soon thereafter, the *Chandra X-ray Observatory* (CXO) made the first detection of the strongest of the predicted O VI KLL features at 22.05 Å from the so called ‘warm absorber’ region of ionized gas around the central source in active galactic nuclei, thought to be a massive black hole [2]. The observation of X-ray absorption from Li-like O VI in the same wavelength region as the emission lines of He-like O VII enabled the simultaneous determination of column densities and, since the two ions do not usually co-exist in a plasma, indicated a composite plasma with widely disparate temperature regimes [1,2].

Present theoretical calculations for the resonance oscillator strengths employ highly resolved relativistic photoionization cross sections with fine structure [6,1]. The quantity of interest is the differential oscillator strength $\frac{df}{d\epsilon}$ that quantitatively relates photoabsorption per unit energy in the bound-bound and the continuum region as [7–9]

$$\frac{df}{d\epsilon} = \begin{cases} \frac{\nu^3}{2z^2} f_{\text{line}} & , \quad \epsilon < I \\ \frac{1}{4\pi^2\alpha a_0^2} \sigma_{\text{PI}} & , \quad \epsilon > I \end{cases} \quad (0.1)$$

where f_{line} is the line absorption oscillator strength, σ_{PI} the photoionization cross section, I the ionization potential, z the ion charge, ν the effective quantum number at $\epsilon = -\frac{z^2}{\nu^2}$ in Rydbergs, and α and a_0 are the fine structure constant and the Bohr radius respectively. In the bound-free region, with autoionizing resonances, the integrated $\frac{df}{d\epsilon}$ yields the effective photoabsorption in terms of σ_{PI} , i.e.

$$\bar{f}_r(J_i \rightarrow J_f) = \int_{\Delta E_r} \left(\frac{df(J_i \rightarrow J_f)}{d\epsilon} \right) d\epsilon = \left(\frac{1}{4\pi^2\alpha a_0^2} \right) \int \sigma_{\text{PI}}(\epsilon; J_i \rightarrow J_f) d\epsilon, \quad (0.2)$$

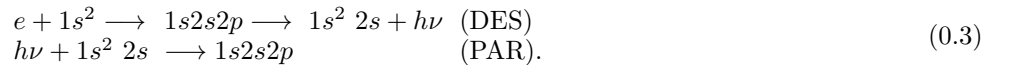
where J_i, J_f are total angular momenta of the initial bound level and the final bound or continuum wavefunction, governed by the usual dipole selection rules $\Delta J = 0, \pm 1; \pi \rightarrow -\pi$. Eq. (0.2) may be evaluated from the detailed σ_{PI} for the $J\pi$ symmetries concerned. However, the resonance profile needs to be sufficiently well delineated and elaborate methods need to be employed to obtain accurate positions and profiles (the background and the peaks) of resonances. Relativistic effects are essential in order to differentiate the fine structure components. We employ

the coupled channel formulation based on the relativistic Breit-Pauli R-matrix (BPRM) method as employed on the extensive work on the Iron Project [10–12].

BPRM photoionization and recombination calculations were reported in earlier works for Li-, He-, H-like carbon and iron: C IV, C V, C VI [13,14] and Fe XXIV, Fe XXV, Fe XXVI [16,15] for applications to X-ray photoionization and non-LTE (NLTE) modeling. We consider the photoionization of the ground level of the Li-like ions C IV, O VI, and Fe XXIV, $1s^2 2s$ ($^2S_{1/2}$) into all $n = 1, 2, 3$ fine structure levels of the He-like ion with $1s^2(^1S_0)$, $1s2s(^3S_1, ^1S_0)$, $1s2p(^3P_{0,1,2}^o, ^1P_1^o)$, $1s3s(^3S_1, ^1S_0)$, $1s3p(^3P_{0,1,2}^o, ^1P_1^o)$ and $1s3d(^3D_{1,2,3}, ^1D_2)$ in the close coupling expansion. Thus K-shell photoionization of the ($1s^2 2s$), i.e. inner-shell excitation-autoionization via the $1s \rightarrow 2p$ transition resulting in $1s2s2p$ (KLL) resonances, is considered with the initial bound state ($^2S_{1/2}$) with symmetry $J = 0.5$ (even parity), and final continua with $J = 0.5$ and 1.5 (odd parity). The six KLL resonances of interest here are: $1s2p(^3P^o)2s$ [$^4P_{1/2,3/2}^o, ^2P_{1/2,3/2}^o$] and $1s2p(^1P^o)2s$ [$^2P_{1/2,3/2}^o$] (the resonances are labeled in Table 1 according to the alphabetical notation by Gabriel [17]). The autoionization and radiative decay rates and cross sections, with and without radiative decay of resonances back to the ground level, are calculated by analyzing the poles in the complex dipole matrix elements using the method described in [16,18]. The cross sections are resolved on a very fine energy mesh of up to 10^{-6} eV.

Whereas calculations have been carried out for C IV, O VI, and Fe XXIV, for brevity we present only the detailed photoionization cross section of the Fe XXIV ground state in Fig. 1 from the L-shell ($2s$) ionization threshold at Fe XXV ($1s^2 ^1S_0$), up to the K-shell ionization thresholds at $1s2s$ and $1s2p$ (marked by arrows in the figure). The top panel (a) presents the σ_{PI} over the extended range with the KLn $n \geq 2$ complexes of resonances KLL, KLM, KLN, etc. (at computed wavelengths) converging on to the K-shell ionization edges. The bottom panel (b) shows the region of KLL resonance complex on an expanded scale, and the strongest resonance (labeled ‘q’, Table 1), fully delineated in (c), showing the orders of magnitude effect of radiation damping. The calculations are further subdivided into the constituent total $J\pi$ symmetries for the ($e + \text{ion}$) continua, and we thereby fully resolve the lowest KLL resonance complex into the six distinct resonance features allowed by the orbital and spin angular momentum couplings, as shown in the bottom panel of Fig. 1. Two sets of cross sections are computed – with and without radiation damping of resonances (solid and dashed lines respectively). It is noted that the Y-scale (Megabarns) in the upper panel is linear, whereas in the bottom panel it is \log_{10} , i.e. the resonance peaks rise orders of magnitude above the nonresonant background. Further, the radiative damping effect attenuates the peak resonance strengths by similarly large amounts, but it is different for each resonance.

These resonances have heretofore been observed in the laboratory as dielectronic satellites (DES) formed via electron-ion excitation of the core ion followed by dielectronic recombination (DR), i.e. radiation damping of the core of the doubly excited autoionization state (e.g Li-like C IV [4]). We may distinguish the DR resonances DES, from the ‘photoabsorption resonances’ (PAR) as:



The PAR’s therefore manifest themselves in photoionization cross sections and photoabsorption spectra, whereas the DES appear in emission spectra. For lighter elements such as C and O, the PAR’s are not likely to be also observed as DES. Thus, in general, resonances may be divided as PAR or DES according to their actual formation and observation depending on plasma conditions in the source. For example, in ions of heavier elements such as Fe XXIV, we expect the same set of resonances to act as PAR’s *or* the DES, and provide useful plasma diagnostics – absorption from cold or cooling environment (with Li-like Fe XXIV for example), or emission at higher temperatures (with DR from He-like Fe XXV). Since both the DES and the PAR are satellite features on the long wavelength side of the resonance lines, they should appear as ‘redward broadening’ of the primary resonance transitions in emission or absorption spectra. This fact may be of considerable astrophysical significance in the analysis of X-ray spectra where such asymmetric broadening of resonance lines is observed, and is sometimes ascribed to relativistic gravitational broadening due to proximity of the plasma source to a massive black hole (see the discussion in Ref. [2]).

Table 1 gives the computed resonance parameters: the associated autoionization and radiative rates (Γ_a, Γ_r), as well as the radiatively undamped (NRD) and the damped (RD) \bar{f}_r ’s for the KLL resonances in C IV, O VI, and Fe XXIV. The \bar{f}_r (NRD) are the conventional f -values, but computed for resonances; the \bar{f}_r (RD) are further multiplied by the ratio of the radiative rate back to the ground level and the sum of all radiative rates. The \bar{f}_r (C IV,NRD) agree well with the length f -values computed in [4] to 3.9% for the $1s2p(^1P^o)2s$, and to 0.9% for the $1s2p(^3P^o)2s$ resonances.

The ‘q’ resonance in Fe XXIV (Fig. 1c) is the narrowest one with an extremely small Γ_a , the lowest among the KLL PAR’s. But it has the largest Γ_r , and hence the largest resonance oscillator strength \bar{f}_r , resulting in the most damped profile. In previous works the resonance Γ_a, Γ_r are generally determined either in the isolated resonance approximation (e.g. [19,20]), or through fitting of complex dipole matrix elements for the dielectronic satellite resonances (e.g. [18,13,16]). The resonances themselves are not fully resolved up to their natural autoionization widths. In the present

work, the ‘q’ resonance required an order of magnitude finer resolution than that needed to derive Γ_a, Γ_r from fitting alone (given in Table 1). The \bar{f}_r ’s obtained from integration over completely resolved $\frac{df}{d\epsilon}$ accounting for all the oscillator strength (as for Fe XXIV), should be somewhat more accurate than from the fits, or isolated resonance approximation when interference between the background and the resonant parts of the wavefunctions is significant. The \bar{f}_r in Table 1 agree very well with those derived from fits to resonances [16]. Another independent check is that the sum over the \bar{f}_r ’s for the KLL resonances of Fe XXIV, 0.782, agrees well with the total absorption oscillator strength in the E1 dipole allowed and intercombination transitions in the core ion Fe XXV $f(1s^2\ ^1S_0 - 1s2p\ ^{(3,1)}P_1^o)$, 0.772.

The present calculations therefore enable not only the calculation of PAR oscillator strengths, but also provide the most stringent check on the accuracy of photoionization calculations. For C IV and O VI all six KLL resonances are not fully delineated due to overlapping and weak components, but the stronger components account for nearly all the expected oscillator strength; the weak components have very small Γ_a and small \bar{f}_r . We should expect the KLL resonances in C IV and O VI to manifest themselves only as PAR’s, and not DES, since the radiative rates are small compared to autoionization rates.

The computed $\frac{df}{d\epsilon}$ for the three ions are shown in Fig. 2, extending from the bound-bound region with the $(2s - np)$ transitions to the bound-free $(2s - \epsilon p)$ in the X-ray region. It may be noted that the bound-bound region is in the UV for C IV and O VI, but in the X-ray for Fe XXIV with the exception of the $n = 2$ transition in the extreme UV. The bound-bound oscillator strengths are computed up to $n = 10$ from the same eigenfunction expansion as in the photoionization and recombination work in Refs. [14,15]; all atomic parameters are thereby obtained in a theoretically self consistent manner. The Fe XXIV and Fe XXV oscillator strengths were reported in Ref. [21] (those for carbon and oxygen ions are as yet unpublished but may be obtained from the first author). The $\frac{df}{d\epsilon}$ are continuous across the ionization threshold, but reflect magnitudes and the structures of discrete and resonant transitions¹. In the bound-bound region the $\frac{df}{d\epsilon}(2s - np)$ is much smaller for $n = 2$ than for $n = 3$, owing to the respective energy differences. The $\frac{df}{d\epsilon}$ therefore rises from $n = 2$ to 3, and then decreases monotonically towards higher n and the first ionization threshold as $n \rightarrow \infty$ ($\epsilon \rightarrow 0$). Fig. 2 presents a complete picture of photoabsorption from the Li-like C IV, O VI and Fe XXIV, from L-shell absorption to the the KLL X-ray features, that should provide plasma diagnostics in two quite different wavelength ranges *from the same ionic species*.

The wavelengths shown in Fig. 2, together with the \bar{f}_r in Table 1, mark the positions and strengths of discrete photoabsorption in the X-ray by Li-like C, O, and Fe. The predicted features and the calculated resonance oscillator strengths \bar{f}_r should be useful in the interpretation of X-ray spectra from the CXO and the *X-ray Multi-Mirror Mission*, and determination of column densities using the standard curve-of-growth method [22]. Further, the significant differences between \bar{f}_r (NRD) and \bar{f}_r (RD), without and with radiative damping, may indicate optical depth effects in the plasma; \bar{f}_r (NRD) is the value to be used in optically thin cases where re-emission following photoabsorption in the resonance along the line of sight is unlikely. More generally, this work demonstrates that resonance photoabsorption spectroscopy can provide information complementary to line emission spectroscopy, and should prove to be a powerful tool for plasma diagnostics, such as for ionization fractions and abundances of elements in astrophysical and laboratory plasmas.

This work was partially supported by the National Science Foundation and the NASA Astrophysical Theory Program. The computational work was carried out at the Ohio Supercomputer Center.

-
- [1] A.K. Pradhan, *Astrophys. J. (Lett.)* **545**, L165 (2000).
 - [2] J.C. Lee *et al.*, *Astrophys. J. (Lett.)* (submitted), astro-ph/0101065.
 - [3] E. Silver *et al.*, *Astrophys. J.* **541**, 495 (2000).
 - [4] S. Mannervik, S. Asp, L. Broström, D.R. DeWitt, J. Lidberg, R. Schuch and K.T. Chung, *Phys. Rev. A* **55**, 1810 (1997).
 - [5] P. Beiersdorfer, T.W. Phillips, K.L. Wong, R.E. Marrs and D.A. Vogel, *Phys. Rev. A* **46**, 3812 (1992).
 - [6] H.L. Zhang and A.K. Pradhan, *Phys. Rev. Lett.* **78**, 195 (1997).
 - [7] M.J. Seaton, *Rep. Prog. Phys.* **46**, 167 (1983).

¹Owing to a typographical error in the plotting routine, $\frac{df}{d\epsilon}(O\ VI, n = 2) = 0.02115$ is incorrectly shown in Fig.2 of Ref. [1] as 0.2115.

- [8] U. Fano and A.R.P. Rau, *Atomic collisions and spectra*, San Diego: Academic Press (1986).
- [9] A.K. Pradhan and H.E. Saraph, *J. Phys. B* **10**, 3365 (1977).
- [10] D.G. Hummer, K.A. Berrington, W. Eissner, A.K. Pradhan, H.E. Saraph and J.A. Tully, *Astron. Astrophys.* **279**, 298 (1993).
- [11] K.A. Berrington, W. Eissner, and P. H. Norrington, *Comput. Phys. Commun.* **92**, 290 (1995).
- [12] Information on the Iron Project and publications is at the following homepages: www.usm.uni-muenchen.de/people/ip/iron-project.html and www.astronomy.ohio-state.edu/~pradhan.
- [13] H.L. Zhang, S.N. Nahar, and A.K. Pradhan, *J. Phys. B* **32**, 1459 (1999).
- [14] S.N. Nahar, A.K. Pradhan, and H.L. Zhang, *Astrophys. J. Suppl.* **131**, 375 (2000).
- [15] S.N. Nahar, A.K. Pradhan, and H.L. Zhang, *Astrophys. J. Suppl.* **32**, xxxx (2001).
- [16] A.K. Pradhan and H.L. Zhang *J. Phys. B* **30**, L571 (1997).
- [17] A. H. Gabriel, *Mon. Not. R. Astron. Soc.* **160**, 99 (1972).
- [18] K. Sakimoto, M. Terao, and K.A. Berrington, *Phys. Rev. A* **42**, 291 (1990).
- [19] L.A. Vainshtein and U.I. Safronova, *At. Data Nucl. Data Tables***25**, 49 (1978).
- [20] F. Bely-Dubau, J. Dubau, P. Faucher and A.H. Gabriel, *Mon. Not. R. Astron. Soc.* **198**, 239 (1982).
- [21] S.N. Nahar and A.K. Pradhan, *Astron. Astrophys. Suppl.* **135**, 347 (1999).
- [22] L. Spitzer, Jr., *Physical Processes in the Interstellar Medium* (New York: Wiley) (1978).

TABLE I. X-ray wavelengths and KLL photoabsorption resonance oscillator strengths for C IV, O VI, and Fe XXIV. Notation $a \pm b$ means $a \times 10^{\pm b}$. The NRD and RD values refer to without and with radiation damping. Γ_a and Γ_r are the autoionization and radiative decay rates respectively.

Resonance	λ_{cal} (Å)	E_r (KeV)	\bar{f}_r NRD (RD)	Γ_a (Ry, s ⁻¹)	Γ_r (Ry, s ⁻¹)
C IV					
$1s2p(^1P^o)2s^2P_{1/2}^o$ (r)	41.42	0.2993	0.3402 (0.3148)	3.24-4, 6.70+12	2.97-5, 6.13+11
$1s2p(^1P^o)2s^2P_{3/2}^o$ (u)	41.42	0.2993	0.1694 (0.1571)	3.18-4, 6.58+12	2.93-5, 6.05+11
$1s2p(^3P^o)2s^2P_{1/2}^o$ (t)	40.94	0.3028	0.0342 (0.0342)	2.75-3, 5.69+13	3.47-6, 7.16+10
$1s2p(^3P^o)2s^2P_{3/2}^o$ (s)	40.94	0.3028	0.0177 (0.0177)	2.75-3, 5.69+13	3.34-6, 6.91+10
O VI					
$1s2p(^1P^o)2s^2P_{1/2}^o$ (r)	22.05	0.5623	0.1924 (0.141)	3.11-4, 6.42+12	1.26-4, 2.60+12
$1s2p(^3P^o)2s^4P_{3/2}^o$ (u)	22.05	0.5623	0.3837 (0.267)	2.76-4, 5.70+12	1.28-4, 2.65+12
$1s2p(^3P^o)2s^2P_{1/2}^o$ (t)	21.87	0.5670	0.0217 (0.0216)	3.41-3, 7.11+13	1.46-5, 3.01+11
$1s2p(^3P^o)2s^2P_{3/2}^o$ (s)	21.87	0.5670	0.0391 (0.0390)	3.43-3, 7.09+13	1.32-5, 2.72+11
Fe XXIV					
$1s2p(^1P^o)2s^2P_{1/2}^o$ (v)	1.873	6.617	2.05-3 (1.61-4)	7.48-6, 1.54+11	1.77-4, 3.66+12
$1s2p(^1P^o)2s^2P_{3/2}^o$ (u)	1.870	6.627	1.42-2 (7.63-4)	3.12-5, 6.45+11	6.38-4, 1.32+13
$1s2p(^1P^o)2s^2P_{1/2}^o$ (r)	1.864	6.649	1.46-1 (1.77-2)	1.89-3, 3.90+13	1.35-2, 2.80+14
$1s2p(^3P^o)2s^4P_{3/2}^o$ (q)	1.860	6.663	4.91-1 (2.58-4)	8.98-6, 1.86+11	2.29-2, 4.74+14
$1s2p(^3P^o)2s^2P_{1/2}^o$ (t)	1.857	6.674	1.10-1 (2.66-2)	3.43-3, 7.10+13	1.04-2, 2.14+14
$1s2p(^3P^o)2s^2P_{3/2}^o$ (s)	1.855	6.681	6.56-3 (6.24-3)	5.12-3, 1.06+14	2.82-4, 5.83+12

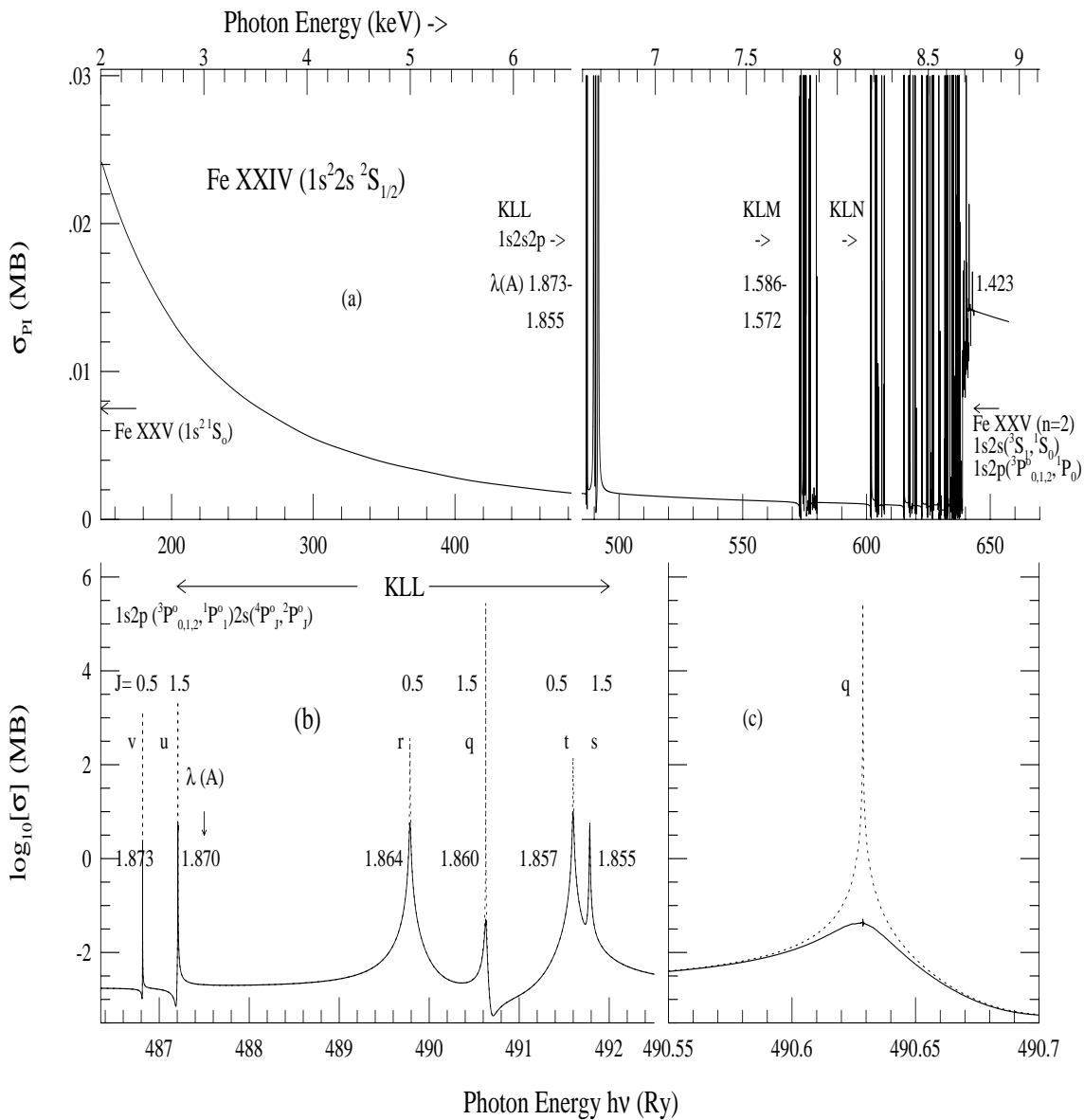


FIG. 1. Ground state photoionization cross section of Fe XXIV with the K-complex of resonances (a), the resolved KLL resonances (b), and completely resolved profile of the q-resonance (c). Note the different energy scales on the X-axis in (a), and in (b) and (c). The upper panel has a linear Y-scale (Megabarns), but the lower panel is on a \log_{10} scale indicating the height of resonances. The large radiation damping of the 'q' resonance (c) is related to its large f_r , stronger than all other resonances.

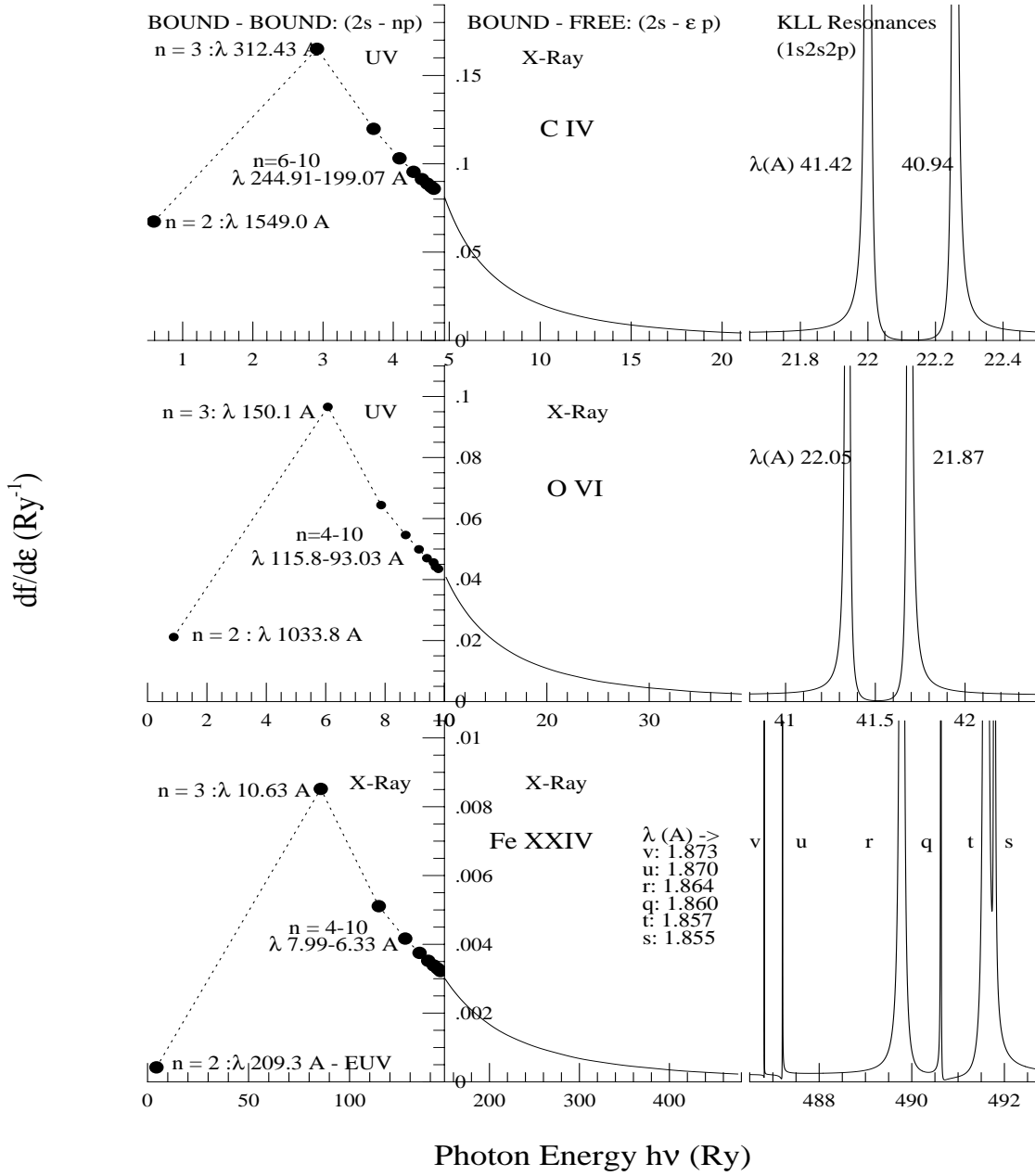


FIG. 2. Differential oscillator strengths $\frac{df}{d\epsilon}$ for C IV, O VI, and Fe XXIV. Wavelengths of the main line and resonance features are marked. The PAR \bar{f}_r 's in Table 1 give the expected strengths in X-ray absorption spectra.